Available online at www.sciencedirect.com
SCIENCE DIRECT®
Journal of Magnetic Resonance 172 (2005) 201–208
JMR Journal of Magnetic Resonance
www.elsevier.com/locate/jmr

EMR and optical study of Mn^{2+} doped potassium trihydrogen selenite

Ram Kripal, Vishal Mishra*

EPR Laboratory, Department of Physics, University of Allahabad, Allahabad 211002, India

Received 19 May 2004; revised 9 September 2004
Available online 13 November 2005

Abstract

The EMR study of Mn^{2+} doped potassium trihydrogen selenite is performed and the site of Mn^{2+} in the lattice is discussed. The zero field parameters providing good fit to the observed EMR spectra are estimated. The spin-Hamiltonian parameters g, A, B, D, and a are (2.0003 ± 0.0002), $(31 \pm 2) \times 10^{-4}$, $(20 \pm 2) \times 10^{-4}$, $(87 \pm 2) \times 10^{-4}$, and $(-9 \pm 1) \times 10^{-4}$ cm^{-1}, respectively. The percentage of covalency of the metal-ligand bond is also determined. The optical absorption study suggests the lattice distortion in the crystal. The electron repulsion and crystal field parameters having good fit to the observed optical spectra are evaluated. The band positions are fitted with the Racah parameters (B and C), the cubic crystal field splitting parameters (Dq), and the Trees correction (α). The values of B, C, Dq, and α are 871, 2967, 670, and 76 cm^{-1}, respectively.

PACS: 76.30
Keywords: Spin-Hamiltonian; Covalency; Electron repulsion parameter; Zero field parameter; Optical spectra

1. Introduction

The EMR technique is used to study paramagnetic ions in host lattices to provide valuable information about the site symmetry of the metal ions [1]. When paramagnetic ions are introduced in host lattices, local distortions will take place due to mismatch of paramagnetic ion size to that of the host ions. The optical study provides energy level ordering of different orbital levels of the paramagnetic ion and crystalline field strength in the host lattice. Thus EMR and optical absorption are two supplementary powerful tools to investigate the site symmetry and associated distortions. EMR of Mn^{2+} has been studied extensively in the investigation of structural and dynamic aspects of crystalline state, since the zero field splittings in these ions are sensitive to even small distortions [2,3] in the lattice.

In the present investigation the EMR and optical study of Mn^{2+} doped $KH_3(SeO_3)_2$ are reported to obtain information whether Mn^{2+} ion enters the lattice substitutionally or interstitially, and to predict the lattice distortion. The study is further used to find the energy level ordering of various orbital levels of the metal ion and the nature of bonding of paramagnetic ion with different ligands.

2. Crystal structure

The crystal structure [4] of $KH_3(SeO_3)_2$ is orthorhombic with unit cell dimensions, $a = 1.6152$, $b = 0.6249$, and $c = 0.6307$ nm, space group P_{bcn} with $Z = 4$. The selenite ions are held together by two OHO bonds and a hydrogen-bonding network exists. The shorter bond involves oxygen atoms related by a twofold symmetry axis and at an O···O distance of 0.2567 nm. Since the longest O···O distance in a symmetric O···H···O bond is about 0.255 nm, it is assumed that the hydrogen

* Corresponding author. Fax: +91 0522 27733863.
E-mail addresses: ram_kripal2001@rediffmail.com (R. Kripal), vishalrohit1@rediffmail.com (V. Mishra).

1090-7807/$ - see front matter © 2004 Elsevier Inc. All rights reserved.
doi:10.1016/j.jmr.2004.09.026

atoms participating in these bonds are statistically distributed in two symmetry-related positions.

3. Experimental

Potassium trihydrogen selenite (PTS) $[KH_3(SeO_3)_2]$ single crystals are grown at room temperature by slow evaporation of an aqueous equimolar solution of selenium dioxide and potassium carbonate. For Mn^{2+} doped crystal, 0.1 wt% of manganese sulphate solution is added as paramagnetic impurity. Good pink coloured crystals are obtained in about 25 days. The EMR spectra of single crystals have been recorded at an interval of 10° in the three orthogonal planes ab, bc, and ca at 77 K (room temperature spectra have insufficient number of lines) on Varian X-band E-112 ESR spectrometer with 100 kHz field modulation. The magnetic field was measured using a proton probe with a Hewlet–Packard frequency counter. Optical absorption spectra have been recorded on Unicam-5625 spectrophotometer at room temperature in the wavelength range 195–1100 nm.

4. Results and discussion

The EMR spectra of Mn^{2+} in PTS at 77 K shows five sets with six lines in each set. This spectrum is characteristic of a system with $S = 5/2$ and $I = 5/2$. A typical EMR (ESR) spectrum recorded when the applied magnetic field B is parallel to the 'a' axis is shown in Fig. 1.

The spin-Hamiltonian for a spin multiplet due to second order effects and other zero-field terms, is given by the following expression [5,6]

$$\begin{aligned}\mathcal{H} &= g\mu_\beta BS + D\{S_z^2 - 1/3S(S+1)\} + E(S_x^2 - S_y^2) \\ &\quad + (a/6)[S_x^4 + S_y^4 + S_z^4 - 1/5S(S+1) \\ &\quad \times (3S^2 + 3S - 1)] + AS_zI_z + B(S_xI_x + S_yI_y) \\ &\quad - \gamma\mu_N BI + Q\{I_z^2 - 1/3I(I+I)\}, \end{aligned} \quad (1)$$

where g is the spectroscopic splitting factor, assumed to be isotropic, μ_β is the Bohr magneton, B is the external field, and S the electron spin operator. The first term represents the electronic Zeeman interaction, second and third terms represent, respectively, the axial and rhombic parts of the fine structure, the fourth term represents the cubic part of the crystal field [7], the fifth and sixth terms represent the hyperfine interaction terms ($I = 5/2$). The seventh and eighth terms represent nuclear Zeeman interaction and quadrupole interaction terms, respectively. The last two terms are too small to produce an observable effect on the spectrum, but they are included for completeness.

In the absence of applied magnetic field, the ground state of Mn^{2+} ion $^6S_{5/2}$ splits into three Kramers doublets with separations of 4D and 2D due to electronic magnetic interaction. These doublets split further [8], by the application of external magnetic field, into six levels with successive separations, $g\beta B + 4D$, $g\beta B + 2D$, $g\beta B$, $g\beta B - 2D$, and $g\beta B - 4D$. Transitions between these levels will give rise to five equally spaced lines, each of which further splits into a sextet due to hyperfine interaction resulting from the nuclear spin of $I = 5/2$. Hence a five set pattern of six components each (i.e., 30 line pattern) is expected.

The allowed transitions and the fields B, at which they occur when Zeeman interaction is dominating, are given by Eq. (A.3) [8].

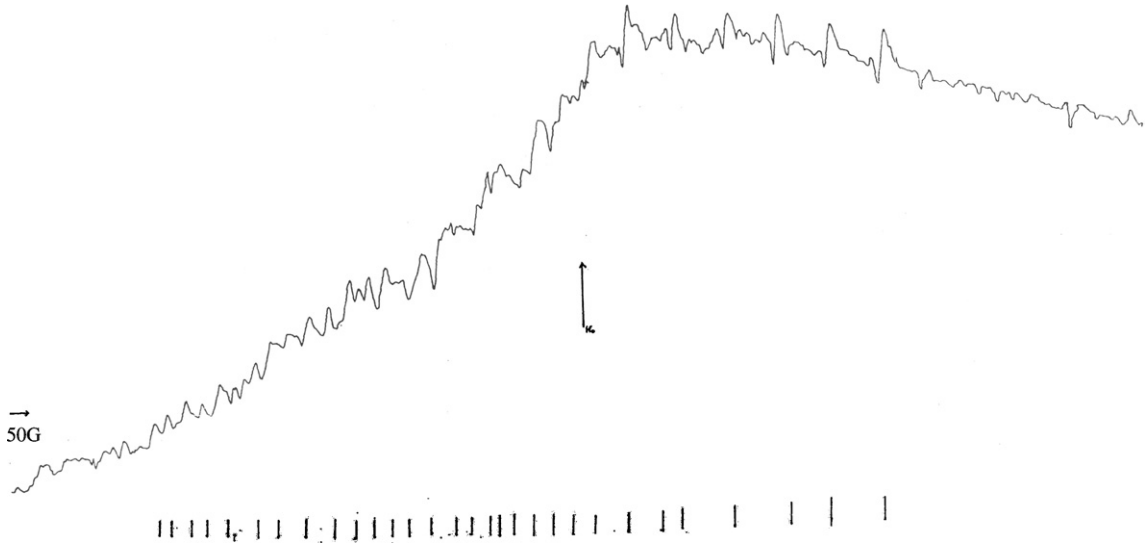

Fig. 1. ESR spectra of Mn^{2+} doped PTS when the applied magnetic field B is parallel to 'a' axis.

Crystal rotations have been carried out in the three orthogonal planes ab, bc, and ca. The angular variation plots of the fine structure in these planes using Eq. (A.3) [8] and experimental record are given in Figs. 2A–C. In all the three planes only one magnetically distinct site is observed. This has been explained on the assumption that Mn^{2+} enters the lattice interstitially.

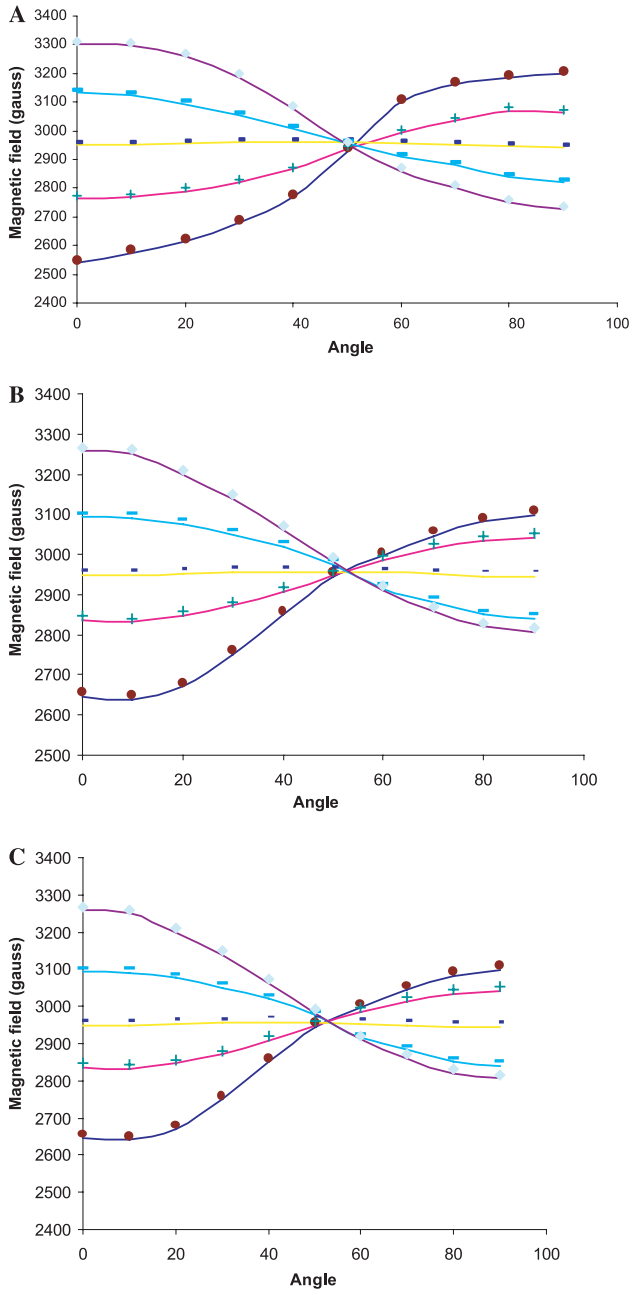

Fig. 2. (A) Angular variation of the fine structure of Mn^{2+} doped potassium trihydrogenselenite in the bc plane (showing the experimental points and the calculated curves). (B) Angular variation of the fine structure of Mn^{2+} doped potassium trihydrogen selenite in the ab plane (showing the experimental points and the calculated curves). (C) Angular variation of the fine structure of Mn^{2+} doped potassium trihydrogenselenite in the ca plane (showing the experimental points and the calculated curves).

Direction cosines of the distortion axis are calculated [9] using the method of Rao and Subramanian and are given in Table 1 along with the direction cosines of some K–O bonds. It is clear from the table that the direction cosines of the distortion axis do not match with any one of the K–O directions. This indicates that Mn^{2+} does not substitute K but enters the lattice interstitially.

The values of g, A, B, D, and a for Mn^{2+} in PTS evaluated using computer program are given in Table 2.

Jain and Venkateswarlu studied EPR of Mn^{2+} doped alkali trihydrogen selenite including PTS. In PTS and rubidium trihydrogen selenite (RTS) they observed only a single line but in case of lithium and sodium trihydrogen selenite they were able to get a good number of lines, sufficient to obtain spin-Hamiltonian parameters. Their values are given in Table 2 for comparison. The crystalline imperfection was given as the cause to the large zero field splittings [10] in these crystals.

The percentage of covalency of the Mn–O bond is also determined [11] from Matamura's plot. The covalency of bond between Mn^{2+} and its ligands will affect the magnitude of the isotropic hyperfine coupling constant [11,12]. The covalency C of a bond between atoms **A** and **B** is approximately related to their electronegativities $\chi_{\mathbf{A}}$ and $\chi_{\mathbf{B}}$ by solving

$$C = [1 - 0.16(\chi_{\mathbf{A}} - \chi_{\mathbf{B}}) - 0.035(\chi_{\mathbf{A}} - \chi_{\mathbf{B}})^2]/n,$$

where n is the number of atoms of neighbour bond. Using the values $\chi_{Mn} = 1.4$ and $\chi_o = 3.5$, the percentage of covalency is found as 23. The value of hyperfine splitting constant $35 \times 10^{-4}\ cm^{-1}$ predicted from the graph also agrees reasonably well with the observed value of $24 \times 10^{-4}\ cm^{-1}$, $(A + 2B)/3$.

Table 1
Direction cosines of K ion with surrounding oxygen; O(1)–O(2) and the distortion axis of Mn^{2+} derived from ESR spectra

Direction	l	m	n
K–Se	±0.9915(5)	±0.0006(5)	±0.0416(5)
K–O(1)	±0.9660(4)	±0.1915(4)	±0.1736(3)
O(1)–O(2)	±0.2750(3)	±0.0135(5)	±0.9658(5)
Distortion axis	±0.2935(4)	±0.0194(3)	±0.9558(5)

Uncertainties are given in brackets.

Table 2
Spin-Hamiltonian parameters for Mn^{2+}in PTS

Spin-Hamiltonian parameters	PTS	$LiH_3(SeO_3)_2$	$NaH_3(SeO_3)_2$
g	2.0003 ± 0.0002	2.009	1.998
A	31 ± 2	86.5	85.1
B	20 ± 2	84.4	82.7
D	87 ± 2	355.5	855.6
a	−9 ± 1	−4.7	−25

A, B, D, and a all in units of $10^{-4}\ cm^{-1}$.

The spin-orbit parameter is regarded [6] as reduced in the solid compared with the free ion. There are two types of matrix elements of orbital angular momentum **L**, those inside the manifold t_2 and those between t_2 and e. Use of the augmented orbital results in multiplication of the t_2 matrix elements by a certain numerical factor $k_{\pi\pi}$ and t_2 and e matrix elements by another factor $k_{\pi\sigma}$. The covalent bonding modifies the spin-orbit coupling in a way which is related to the reduction of the orbital angular momentum through the coefficients $k_{\pi\pi}$ and $k_{\pi\sigma}$.

The deviations $\Delta g = g - 2.0023$ are observed in compounds where a fair amount of covalent bonding (or a decrease in ionicity) would be expected. It has been suggested [13] that in the presence of covalent bonding excited sextets $^6T_{1g}$ are present, whose single electron states will tend to be full or empty according to whether electrons are transferred to or from the central ion by the bonding action. A second-order shift is then possible in the g value, whose sign depends on the direction of electron transfer. The value $-.0020$ of Δg in our case is consistent with this picture.

5. Optical spectra

In a cubic crystalline field of moderate strength [14] Mn^{2+} $3d^5$ electrons are distributed in the t_{2g} and e_g orbitals. Thus the ground state configuration is written as $(t_{2g})^3 e_g^2$. This configuration gives rise to the electronic states $^6A_{1g}$, $^4A_{1g}$, ^4E_g, $^4T_{1g}$, $^4T_{2g}$, and $^4A_{2g}$ and to a number of doublet states. The $^6A_{1g}$ lies lowest and is the ground state. The other excited electronic configuration like $(t_{2g})^4$ e_g, $(t_{2g})^2 e_g^3$, and $t_{2g} e_g^4$ give rise to several doublet and quartet states. Thus all the absorption bands of high spin Mn^{2+} result from spin forbidden transitions.

The observed optical absorption spectrum at room temperature is shown in Figs. 3 and 4. The spectrum consists of seven main bands located at 19,557, 21,258, 23,036, 24,050, 26,730, 29,137, and 32,950 cm^{-1}. In addition to the above, two weak bands at 24,060, 25,610 cm^{-1} are observed. Similar weak bands were also reported at room temperature by several authors [15–18]. Among the bands observed in the present studies, the band at 23,036, 24,050, and 29,137 cm^{-1} are found to be sharp. Ligand field bands are sharp when the energy expressions for the transition are independent of Dq, because the number of t_{2g} electrons is the same in both the excited and ground states [14]. The two states $^4A_{1g}(G)$ and $^4E_g(G)$ are normally degenerate, but their degeneracy is often lifted by covalency in the crystal [19]. According to earlier workers [20,21] any of the $^4A_{1g}(G)$ and $^4E_g(G)$ levels could lie lower depending upon a judicious choice of the various covalency parameters. In fact the position of the $^4E_g(G)$ state is influenced by the interaction with the $^4E_g(D)$ state while the position of $^4A_{1g}(G)$ is not affected. Thus the $^4E_g(G)$

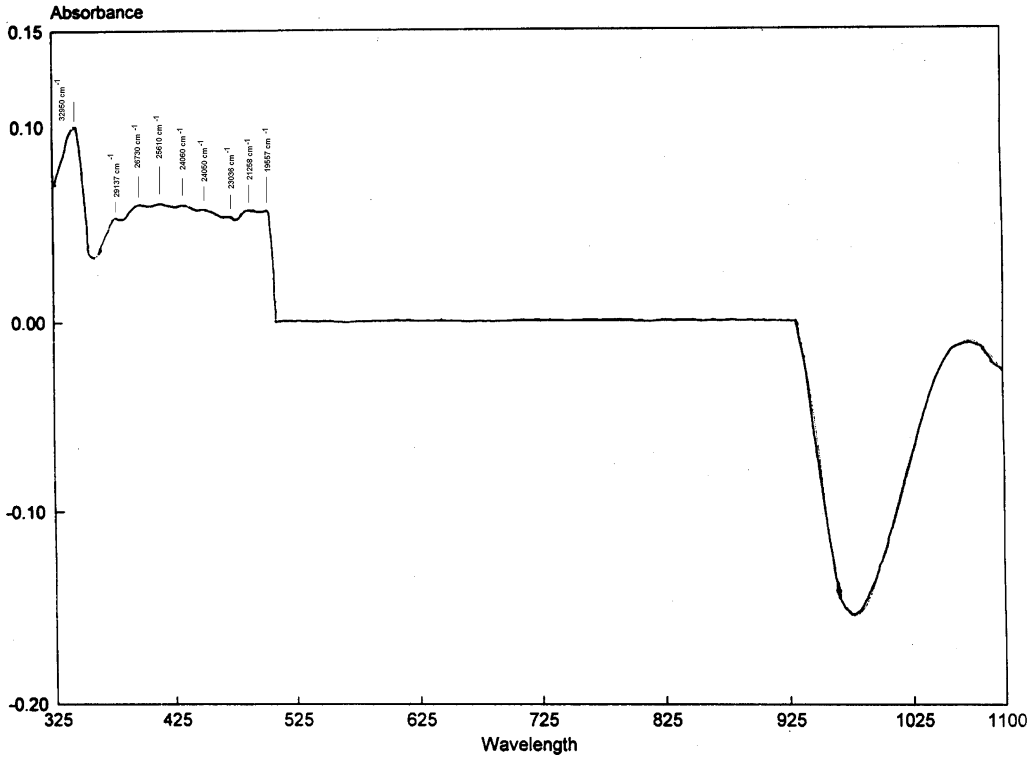

Fig. 3. Absorption spectrum of Mn^{2+} in potassium trihydrogen selenite in the wavelength range 325–1100 nm.

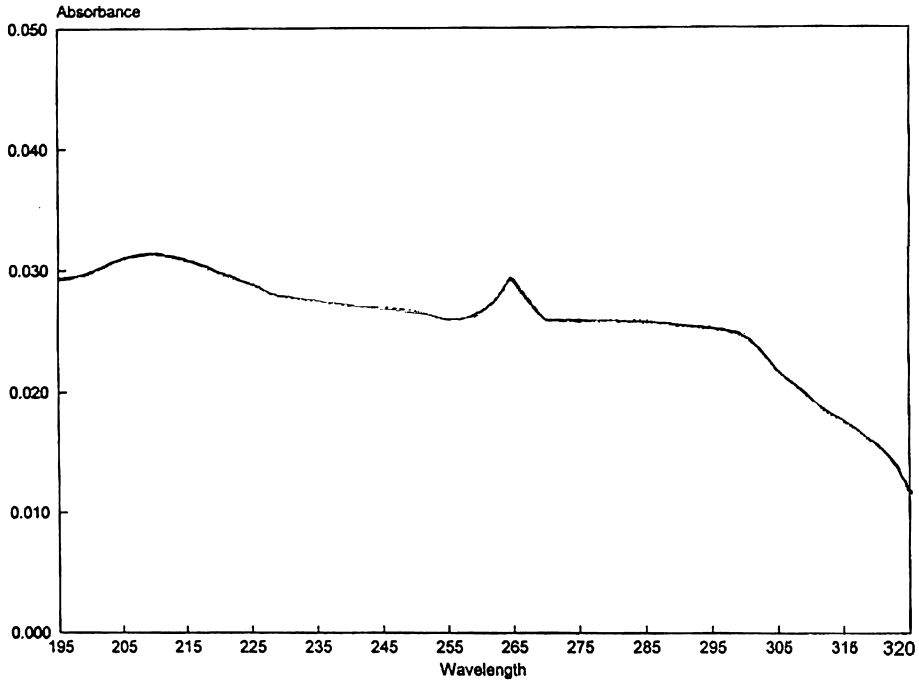

Fig. 4. Absorption spectrum of Mn^{2+} in potassium trihydrogen selenite in the wavelength range 195–325 nm.

level should be affected more by slight changes in the environment in different crystals as compared with the $^4A_{1g}(G)$ level. Therefore the bands at 23,036, 24,050 cm^{-1}, are attributed to the states $^4E_g(G)$ and $^4A_{1g}(G)$, respectively. The third sharp band at 29,137 cm^{-1} is assigned to the transition $^6A_{1g}(S) \rightarrow {}^4T_{1g}(P)$. Using the Tanabe–Sugano diagram [22] the other bands at 19,557, 21,258, 26,730, and 32,950 cm^{-1} are assigned to $^4T_{1g}(G)$, $^4T_{2g}(G)$, $^4T_{2g}(D)$, and $^4T_{1g}(P)$ states, respectively. The wavelengths and the wave numbers of the bands are given in Table 3, together with the assignments.

The energy levels are calculated using the Racah parameters (B and C), the cubic crystal field splitting parameter (Dq) and the Trees correction (α) [22]. The correction term is relatively small, and so it is arbitrarily fixed at the free ion value of 76 cm^{-1}. The energy matrices including Trees correction have been given Mehra [23].

The electrostatic parameters B and C are evaluated from the energy states $^4E_g(G)$ and $^4E_g(D)$, which are independent of Dq.

Once the assignments of the bands of the spectrum have been made, the values of B and C are then used in solving the secular equations of Mehra [23] to evaluate a single value of Dq.

The energy values for quartet electronic states have been calculated using computer for different values of Dq with $B = 871$ cm^{-1}, $C = 2967$ cm^{-1}, and $\alpha = 76$ cm^{-1}. A good fit of the experimentally observed band positions is obtained for $Dq = 670$ cm^{-1} as is seen from the graph in Fig. 5.

It is interesting to note that the observed and calculated values are in good agreement, justifying the assignments.

Experimental evidence for a reduction of the electrostatic parameters B and C in octahedral complexes is given by Owen and Thornley [24]. The parameters B and C are reduced considerably from those of the free ion value because of covalent bonding [25,26].

For a given element the magnitude [27] of the total inter-electronic repulsion may be measured by the accumulative parameter ρ given by

$$\rho = (D^2 + E^2)^{1/2},$$

Table 3
The experimental data and the analysis of the absorption spectrum of Mn^{2+} ions in potassium trihydrogen selenite

Transition from $^6A_{1g}(S)$	Observed (nm)	Observed (cm^{-1})	Calculated (cm^{-1})
$^4T_{1g}(G)$	511.3	19,557(20)	19,542
$^4T_{2g}(G)$	470.4	21,258(15)	26,510
$^4E_g(G)$	434.1	23,036(10)	23,085
	415.8	24,050(9)	24,080
$^4A_{1g}(G)$	415.6	24,060 (7)	
	390.4	25,610(7)	
$^4T_{2g}(D)$	374.1	26,730(15)	26,710
$^4E_g(D)$	343.2	29,137(12)	27,108
$^4T_{1g}(P)$	334.0	32,950(8)	32,942

$B = 871$ cm^{-1}, $C = 2967$ cm^{-1}, $Dq = 670$ cm^{-1}, and $\alpha = 76$ cm^{-1}. Uncertainties are given in brackets.

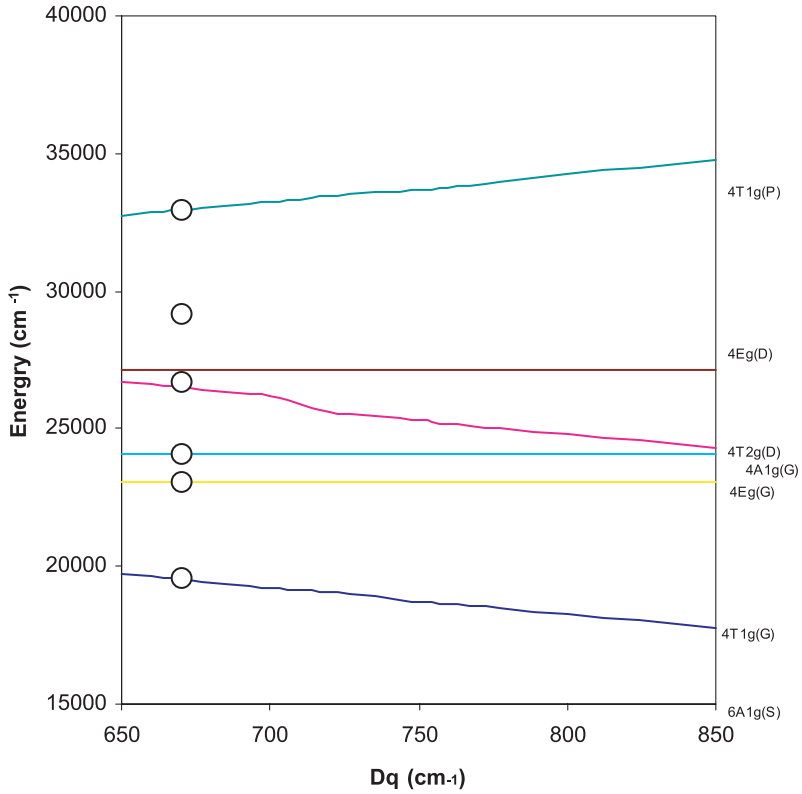

Fig. 5. The energy level diagram of Mn^{2+} in a cubic field showing the variation of the levels vs Dq with $B = 871\ cm^{-1}$, $C = 2967\ cm^{-1}$, and $\alpha = 76\ cm^{-1}$ (the circles show the experimental energies).

where D, the spin-pairing energy parameter is a measure of the energy differences between the barycentres of the different spin multiplicities of a configuration

$$D = 7/6[(5/22)B + C]$$

and the parameter E measures the energy separation between the terms of the highest spin multiplicity for the configurations that contain more terms of this kind.

$$E = (21/4)B.$$

The parameter ρ decreases with decreasing ionic charge due to the expansion of the d shell. By this expansion the average distance between the d electrons is increased while the average reciprocal distance, directly reflecting the repulsion, is decreased.

Gabriel et al. [28] found possible to fit both the observed value of cubic splitting parameter a for Mn^{2+} in MgO and the optical spectrum of MnO, using rather smaller values of single electron spin-orbit coupling $\zeta < 300\ cm^{-1}$. In the range $+1000\ cm^{-1} \leqslant Dq \leqslant +1500\ cm^{-1}$ the parameter a was found to be a sensitive function of ζ and Dq, varying approximately as ζ^4 and $(Dq)^n$, where n varies between 3.5 and 6.

The free ion value of the Racah parameters B and C are 960 and 3325 cm^{-1}, respectively [24,29]. In the present study, we obtained the value of $B = 871$ and $C = 2967\ cm^{-1}$. The considerable decrease in the value of the Racah electron repulsion parameters B and C (from 960 to 871 cm^{-1}, 3325 to 2967 cm^{-1}) may be due to covalent bonding [24,25] between the central metal ion and the ligand.

It can be seen from the crystal structure [4] that there are two cation sites (K^+ and Se^{6+}) available to the Mn^{2+} ion for substitution. The ionic radii of K^+, Se^{6+}, and Mn^{2+} are 0.133, 0.042, and 0.080 nm [30], respectively. Because of the large differences in the ionic radii and the valence states of the two ions, Mn^{2+} does not properly fit in at the Se^{6+} site. On the other hand it also does not seem fit well at the K^+ site due to large difference between the ionic radii of the two ions though there is only a small difference in their valence states. Moreover, the introduction of Mn^{2+} in place of K^+ ion in the lattice will cause a charge imbalance and the neutrality of the crystal will then have to be maintained by the formation of positive ion vacancies. However, if it is assumed that Mn^{2+} ion enters the lattice substitutionally in place of K^+ then one can expect four magnetically distinct sites per unit cell as the PTS contains four potassium atoms in the unit cell [4]. But in the present investigation only one set of allowed hyperfine lines is observed in all the three planes of rotation and hence the possibility of Mn^{2+} ion entering the lattice substitutionally is ruled out. The other possibility is interstitial site. The direction cosines of the distortion axis calculated in the present investigation nearly coincides with the direction of O (1)–O (2) bond. Therefore the Mn^{2+} ions may be

expected to occupy the distorted octahedral interstitial site in PTS.

6. Conclusions

The EMR study of Mn^{2+} doped PTS has been carried out at 77 K. The spin-Hamiltonian parameters g, A, B, D, and a have been determined. From these results, the Mn^{2+} ions may be expected to occupy the distorted octahedral interstitial site in PTS. The optical absorption study has been carried out at room temperature and the bands observed have been assigned to transitions from the ${}^6A_{1g}(S)$ ground state to various excited levels of Mn^{2+} ion in cubic crystalline field. The observed band positions have been fitted with four parameters B, C, Dq, and α. The covalency of the metal ligand bond has also been discussed.

Acknowledgment

One of the authors (Vishal Mishra) is grateful to Council of Science and Technology, U.P. (India) for financial support.

Appendix A. Calculation of Racah parameters

The energy matrix for ${}^4E_g(G,D)$ is:

$$\begin{vmatrix} -22B+5C+12\alpha-E & -2\sqrt{3}B+4\sqrt{3}\alpha \\ -2\sqrt{3}B+4\sqrt{3}\alpha & -21B+5C+14\alpha-E \end{vmatrix} = 0. \tag{A.1}$$

The energy for the ground state ${}^6A_{1g}(S)$ is $-35B$.

Substituting $E=-35B+T$ in above we have

$$\begin{vmatrix} 13B+5C+12\alpha-T & (-2B+4\alpha)\sqrt{3} \\ (-2B+4\alpha)\sqrt{3} & 14B+5C+14\alpha-T \end{vmatrix} = 0. \tag{A.2}$$

Solving the above matrix, we get

$$T=1/2\left[(27B+10C+26\alpha)\pm\sqrt{49B^2-188B\alpha+196\alpha^2}\right]. \tag{A.3}$$

The solution for the above equation is

$$T_1=1/2\left[(27B+10C+26\alpha)-\sqrt{49B^2-188B\alpha+196\alpha^2}\right], \tag{A.4}$$

$$T_2=1/2\left[(27B+10C+26\alpha)+\sqrt{49B^2-188B\alpha+196\alpha^2}\right],$$

$$(T_2-T_1)^2=[49B^2-188B\alpha+196\alpha^2], \tag{A.5}$$

$$B=\left(94\alpha\pm\sqrt{49(T_2-T_1)^2-768\alpha^2}\right)\Big/49. \tag{A.6}$$

In the above expression we always take the positive value of the square root and so

$$B=\left(94\alpha+\sqrt{49(T_2-T_1)^2-768\alpha^2}\right)\Big/49. \tag{A.7}$$

Assuming $188\sim196$, we have from Eq. (A.3)

$$T=1/2[(27B+10C+26\alpha)\pm(7B-14\alpha)], \tag{A.8}$$

$$T_1=10B+5C+20\alpha={}^4E_g(G), \tag{A.9}$$

$$T_2=17B+5C+6\alpha={}^4E_g(D).$$

Thus,

$$C=(T_1+T_2-27B-26\alpha)/10. \tag{A.10}$$

We have taken T_1 as ${}^6A_{1g}(S)\rightarrow{}^4A_{1g}(G)$, ${}^4E_g(G)$ and T_2 as ${}^6A_{1g}(S)\rightarrow{}^4E_g(D)$ since the energy states ${}^4A_{1g}(G)$, ${}^4E_g(G)$ are normally degenerate.

References

[1] B. Aktas, S. Guner, F. Yildiz, A. Nateprov, A. Siminel, L. Kulyuk, ESR study on Cr^{3+} and Mn^{2+} doped $ZnAl_2S_4$ single crystal, J. Mag. Magn. Mat. 258 (2003) 409–412.
[2] J. Prohaska, M. Tromel, H. Rager, EPR study of Fe^{3+} and Mn^{2+} in CeO_2 and ThO_2, Appl. Magn. Reson. 5 (1993) 387–398.
[3] B.R. Mc Garvey, Transition Metal Chemistry, Ed. By R.L. Carlin 3 (1966) 89.
[4] B. Prelesnik, R. Herak, Lj. Manojlovic-Muir, K.W. Muir, A neutron diffraction study of potassium trihydrogen selenite, $KH_3(SeO_3)_2$, Acta Cryst. B 28 (1972) 3104.
[5] C. Rudowicz, Concept of spin Hamiltonian, forms of zero field splitting and electronic Zeeman Hamiltonians and relations between parameters used in EPR. A Critical Review, Magn. Reson. Rev. 13 (1987) 1–89.
[6] A. Abragam, B. Bleaney, EPR of Transition Ions, Clarendon Press, Oxford, 1970.
[7] C. Rudowicz, H.W.F. Sung, Can the electron magnetic resonance (EMR) techniques measure the crystal (ligand) field parameters? Phys. B 300 (2001) 1–26.
[8] B. Bleaney, D.J.E. Ingram, The paramagnetic resonance spectra of two salts of manganese, Proc. R. Soc. A 205 (1951) 336–356.
[9] P.S. Rao, S. Subramanian, Single crystal EPR studies of some first-row transition ions in hexaimidazole zinc(II) dichloride tetrahydrate,IV.Mn(II): a case of twinning, Mol. Phys. 54 (1985) 429–438.
[10] V.K. Jain, P. Venkateswarlu, Electron paramagnetic resonance of Mn^{2+} doped in alkali trihydrogen selenite single crystals, Can. J. Phys. 56 (1978) 807–813.
[11] O. Matamura, ESR of Mn-activated phosphors, J. Phys. Soc. Japan 14 (1959) 108.
[12] E. Simanek, K.A. Muller, Covalency and hyperfine structure constant A of iron group impurities in crystals, J. Phys. Chem. Solids 31 (1970) 1027–1040.
[13] H. Watanabe, g-value of Fe^{3+} in II-VI cubic crystals, J. Phys. Chem. Solids 25 (1964) 1471–1475.
[14] C.J. Ballhausen, Introduction to Ligand Field Theory, McGraw-Hill, New York, 1962.
[15] A. Mehra, Optical absorption of Mn^{2+} doped alkali halide, Phys. Stat. Solids B 29 (1968) 847–857.
[16] J.P. Srivastava, Electron spectrum of NaF:Mn^{2+}, J. Phys. Chem. Solids 36 (1975) 727–730.

[17] A. Mehra, P. Venkateswarlu, Absorption spectrum of $RbMnF_3$, J. Chem. Phys. 47 (1967) 2334–2342.
[18] J.P. Srivastava, A. Mehra, Optical absorption of $NaMnF_3$, J. Chem. Phys. 57 (1972) 1587–1591.
[19] J. Ferguson, E.R. Krausz, H.J. Guggenheim, High-resolution MCD spectroscopy of transition metal ions in fluoride crystals, The $^6A_{1g} \rightarrow {}^4A_{1g}$, $^4E_g(G)$ no-phonon transitions of Mn^{2+} in $KMgF_3$ and $KZnF_3$, Mol. Phys. 27 (1974) 577–591.
[20] A. Mehra, P. Venkateswarlu, Absorption spectrum of manganese acetate tetrahydrate, J. Chem. Phys. 48 (1968) 4381–4383.
[21] L.L. Lohr Jr., Optical spectra of divalent manganese salts. I. Energy levels for cubic and lower-symmetry complexes, J. Chem. Phys. 45 (1966) 3611–3622.
[22] Y. Tanabe, S. Sugano, On the absorption spectra of complex ions.I., J. Phys. Soc. Japan 9 (1954) 753–766.
[23] A. Mehra, Trees correction matrices for d^5 configuration in cubic symmetry, J. Chem. Phys. 48 (1968) 4384–4386.
[24] J. Owen, J.H.M. Thornley, Covalent bonding and magnetic properties of transition metal ions, Rep. Prog. Phys. 29 (1966) 675–728.
[25] W. Low, G. Rosengarten, The optical spectrum and ground-state splitting of Mn^{2+} and Fe^{3+} ions in the crystal field of cubic symmetry, J. Mol. Spectroc. 12 (1964) 319–346.
[26] M. Dvir, W. Low, Paramagnetic resonance and optical spectrum of iron in beryl, Phys. Rev. 119 (1960) 1587–1591.
[27] M. Broson, C.E. Schaffer, Orthonormal interelectronic repulsion operators in the parametrical d^q model. Application of the model to gaseous ions, Inorg. Chem. 27 (1988) 2522–2530.
[28] J.R. Gabriel, D.F. Johnston, M.J.D. Powell, A calculation of the ground-state splitting for Mn^{2+} ions in a cubic field, Proc. R. Soc. A 264 (1961) 503–515.
[29] B.N. Figgis, Introduction to Ligand Fields, Wiley, New York, 1976, p. 52.
[30] R.C. West, Handbook of Chemistry and Physics, fiftysixth ed., CRC Press, Cleveland, OH, 1975-1976.